Journal of computer science and software applications
https://www.mfacademia.org/index.php/jcssa
ISSN:2377-0430
Vol. 5, No. 3, 2025

AI-Assisted Numerical Analysis of Gasket Deformation and Contact Stress in Shield Tunnel Waterproofing Systems

Cyril Elverson[1], Fenglin Luo[2]
University of Oslo, Oslo, Norway[1],University of Oslo, Oslo, Norway[2]
cyril.elverson@uio.no[1], luofll8891@gmail.com[2]

Abstract:

Waterproofing in shield tunnels is critical for ensuring structural integrity and long-term durability, especially in large-diameter tunnels where joint and segment waterproofing play essential roles. This study employs a combination of numerical simulations and AI-assisted analysis to evaluate the deformation characteristics and contact stress distribution across six gasket cross-section designs. Through finite element analysis (FEA) and machine learning-driven pattern recognition, this research identifies key deformation behaviors and stress concentration areas. Results demonstrate that, under identical hardness conditions, the contact stress at the gasket-gasket interface has the most significant impact on waterproofing performance, surpassing the gasket-pad and gasket-groove interfaces. Section A exhibits optimal waterproofing capability and stable contact stress growth, making it the preferred design for engineering applications. The incorporation of AI techniques further enhances the prediction accuracy and design optimization process, providing a data-driven framework for improving gasket designs in shield tunnel systems.

Keywords:

Shield Tunnel; Joint Waterproofing; Elastic Gasket; Numerical Simulation; Mooney-Rivlin Model; AI-assisted Analysis; Contact Stress Prediction.

1. Introduction

Shield tunnel waterproofing covers segment structure sealing, joint waterproofing, and hand hole sealing, all of which are essential to ensure tunnel durability and safety. In recent years, super-large diameter shield tunnels in China, such as the Wuhan Yangtze River Tunnel[1], Chongming Yangtze River Tunnel[2], Nanjing Weisan Road Yangtze River Tunnel[3-4], Nanjing Metro Airport Line, and Guangzhou Deep Drainage Tunnel, have adopted elastic gaskets tailored to specific engineering needs. The cross-sectional design of these gaskets is typically determined through closed compression force tests and waterproof capacity evaluations.

Zhong Xiaochun and Wu Zhenzhi[5-6]investigated the long-term waterproofing performance of elastic gaskets during the tunnel service cycle using stress relaxation tests. Gong Chenjie et al.[7]summarized the design methodology for elastic gasket cross-sections in large-diameter shield tunnel joints, and successfully applied their findings to the Nanjing Weisan Road Yangtze River Tunnel. Numerical simulation methods, increasingly enhanced with AI-assisted optimization techniques, are now employed to refine gasket section designs, enabling more accurate performance predictions and design adjustments based on multi-scenario simulations.

2. Waterproof Mechanism of Elastic Gasket

The waterproofing performance of elastic gaskets primarily depends on the contact stress generated at the rubber-concrete and rubber-rubber interfaces. During compression, the gasket generates contact stress at the interface with both the adjacent gasket and the concrete segment. Water penetration mainly occurs along two potential paths: (1) between adjacent gaskets and (2) between the gasket and the segment.

If external water pressure exceeds the peak contact stress along these paths, gaps will form, leading to water leakage and gasket failure. The path with the lowest peak contact stress is referred to as the "control path," which acts as the weak point governing overall waterproofing performance. AI-based stress prediction models can now be used to identify such control paths in advance, enabling targeted design improvements to ensure peak contact stress exceeds expected water pressure.

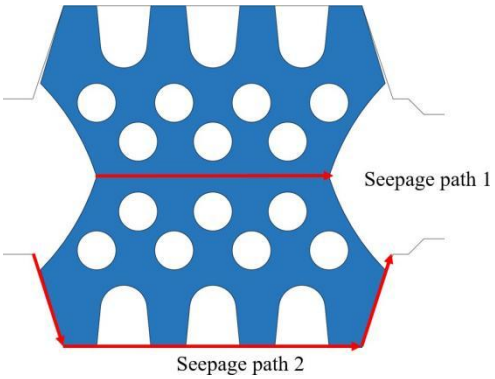

Figure 1. Seepage path

3. Elastic Sealing Gasket Section Form

The cross-sectional shape of elastic gaskets plays a crucial role in determining their waterproof performance. Commonly used cross-sectional types include trapezoidal, comb, and middle-hole designs. Trapezoidal sections are typically used in water-swelling rubber gaskets. Comb-shaped sections, composed of multiple evenly spaced teeth, are commonly found in elastic rubber gaskets, offering higher compression ratios compared to trapezoidal sections of equivalent skeleton area.

Middle-hole sections are modified comb designs with enclosed internal holes. These holes can take triangular, rounded, or irregular shapes to suit various performance requirements. Middle-hole sections are now the mainstream choice for both elastic and water-swelling rubber gaskets due to their adaptability.

To address leakage risks at the contact points between traditional gaskets and concrete segments, some shield tunnels now adopt embedded gaskets. These are prefabricated into the segment itself, with both sides of the gasket directly embedded into the segment, enhancing installation precision and waterproofing reliability. AI-driven shape optimization algorithms can further refine these sections by correlating cross-sectional geometries with stress distribution patterns under different working conditions.

4. Section Design of Elastic Gasket

The dimensions of the gasket groove are shown in Figure 2. The groove depth is 12 mm, with a cross-sectional area of 615 mm². The optimal gasket cross-sectional area should range from 535 to 615 mm².

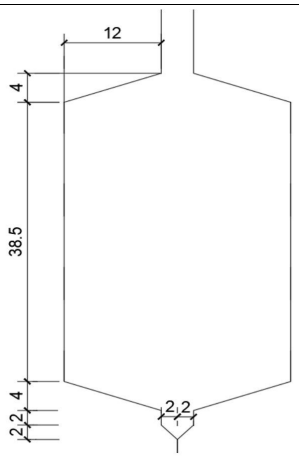

Figure 2. Seal gasket groove diagram (unit : mm)

Based on the groove size, engineering constraints, and accumulated project experience, six candidate gasket section designs (A to F) were proposed, as shown in Figure 3. The interface parameters for each section, including area, opening ratio, and effective compression area, are summarized in Table 1. AI-based clustering and multi-objective optimization were applied to pre-screen these designs for stress distribution uniformity and waterproofing performance before detailed numerical simulation.

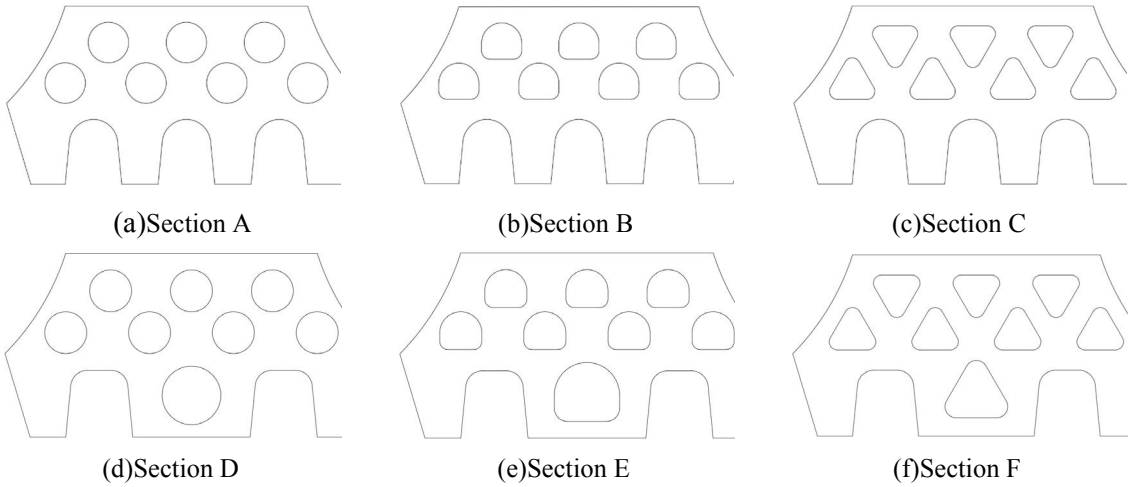

Figure 3. Sealing gasket section diagram

Table 1: Sealing gasket section parameter table

Section	Groove area /mm^2	Outer contour area/mm^2	Closed hole area /mm^2	Open hole area /mm^2	Net area/mm^2	Opening rate	Groove area /Net area
A	615	846.43	137.45	140.13	568.86	0.328	1.081
B	615	846.43	135.72	140.13	570.58	0.326	1.078
C	615	846.43	138.42	140.13	567.89	0.329	1.083
D	615	846.43	175.93	112.84	557.66	0.341	1.103
E	615	846.43	182.37	112.84	551.22	0.349	1.116
F	615	846.43	174.45	112.84	559.14	0.339	1.100

5. Finite Element Model of Elastic Gasket

5.1 Material Constitutive and Parameters

EPDM material is usually regarded as isotropic incompressible hyperelastic material. The nonlinear

stress-strain constitutive relation of hyperelastic materials is mainly defined by strain energy function. The commonly used Mooney-Rivlin two parameter model is used in the calculation, and the strain energy function is expressed as

$$W = C_{10}(I_1 - 3) + C_{01}(I_2 - 3)$$

According to the above formula, the Mooney-Rivlin model parameters of rubber materials with different hardness were calculated, as shown in Table 2.

Table 2: Mooney-Rivlin model parameter values of rubber materials with different hardness

Shore hardness of rubber /HA	Elastic modulus /MPa	C_{10}/MPa	C_{01}/MPa
55	2.978	0.397	0.099
60	3.619	0.483	0.121
65	4.443	0.592	0.148
70	5.542	0.739	0.185

In this section, EPDM with hardness of 70 was used in numerical simulation.

5.2 Establishment of Finite Element Model

The finite element model of the EPDM elastic gasket was developed using ABAQUS/Explicit, as shown in Figure 4. In practical engineering applications, the segment gasket groove is typically made of concrete, whose stiffness is significantly higher than that of the elastic gasket. Consequently, the gasket groove is modeled as an analytical rigid body, ensuring that the groove does not undergo any deformation during the simulation process.

To facilitate loading and boundary condition application, a reference point is assigned to the groove component. The compression deformation between gaskets is simulated by applying a displacement at this reference point, controlling the relative compression between adjacent gaskets.

Considering that the longitudinal dimension of the gasket is much greater than its width, the gasket is modeled using plane strain elements, which appropriately reflect the two-dimensional stress state across the cross-section. The simulation employs explicit dynamic algorithms to accurately capture the contact interaction, large deformation behavior, and non-linear material responses of the gasket under compression. Additionally, AI-based contact analysis enhancement techniques could be incorporated in future studies to improve contact stress convergence and predict potential local failure zones based on historical simulation data.

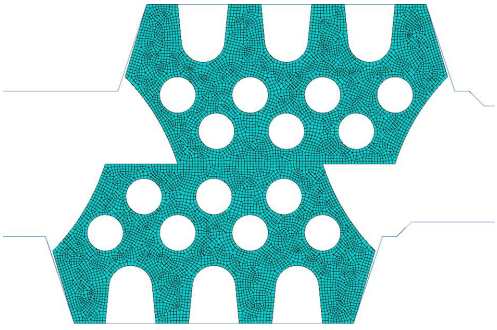

Figure 4. Numerical model of gasket

6. Elastic Gasket Section Optimization

In this section, the deformation characteristics of the six designed sections after compression

deformation are discussed by numerical simulation method, and the deformation characteristics of the open and closed holes when the six sections change with the opening amount are analyzed.

6.1 Deformation Characteristics of Gaskets with Different Cross-Section Forms

In this section, the opening amount of the gasket is controlled by applying a displacement load to the segment, and the extrusion deformation process of the gasket in the actual assembly process of the project is simulated. The deformation characteristics of the gasket under the conditions of 6 kinds of cross-sections in the dislocation of 0mm, rubber hardness of 70, opening of 0,4,8 are shown in Figure 5-Figure 10.

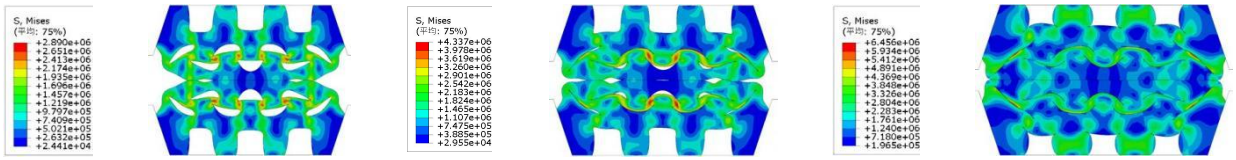

(a) Opening amount 8mm (b)Opening amount 4mm (c)Opening amount 0mm

Figure 5. Section A gasket deformation stress nephogram

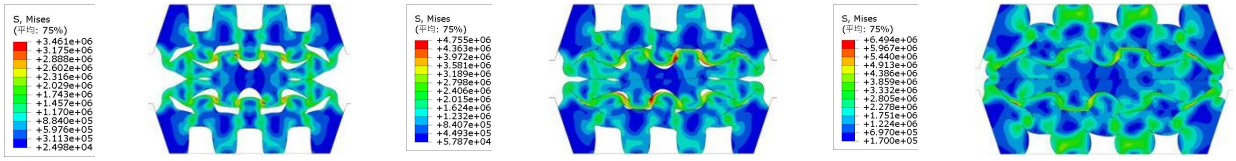

(a)Opening amount 8mm (b)Opening amount 4mm (c)Opening amount 0mm

Figure 6. Section B gasket deformation stress nephogram

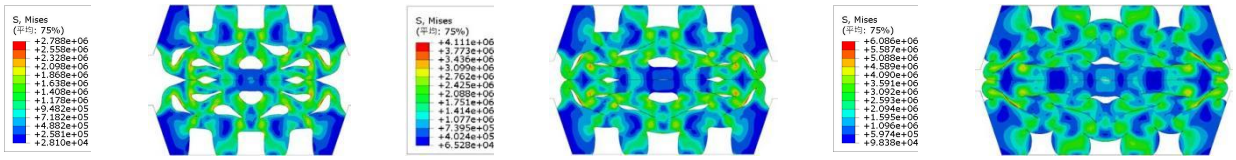

(a)Opening amount 8mm (b)Opening amount 4mm (c)Opening amount 0mm

Figure 7. Section C gasket deformation stress nephogram

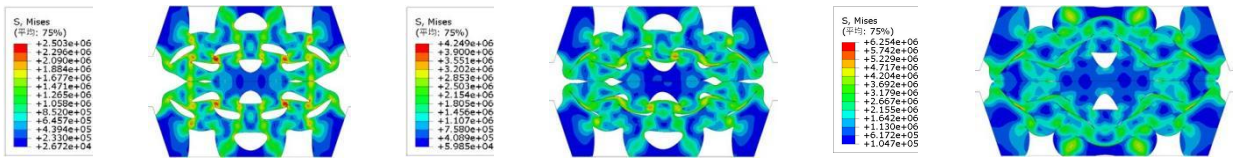

(a)Opening amount 8mm (b)Opening amount 4mm (c)Opening amount 0mm

Figure 8. Section D gasket deformation stress nephogram

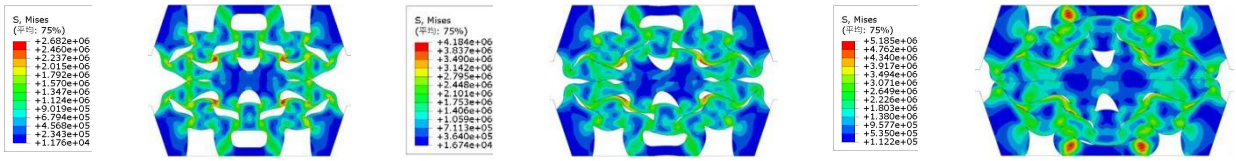

(a)Opening amount 8mm (b)Opening amount 4mm (c)Opening amount 0mm

Figure 9. Section E gasket deformation stress nephogram

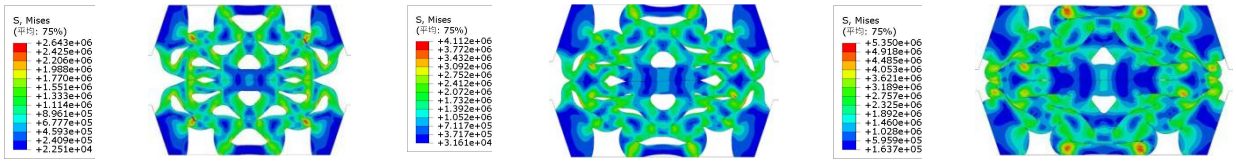

(a)Opening amount 8mm (b)Opening amount 4mm (c)Opening amount 0mm

Figure 10. Section F gasket deformation stress nephogram

As shown in Fig.5-Fig.10, when the opening amount is 8mm, the internal holes begin to compress initially, while the shape of the open holes remains good, and the teeth at the bottom of the gasket are basically not deformed. When the opening amount is 4mm, the closed hole and the open hole of the gasket are further compressed. The closed hole is basically completely compressed and dense, with a small amount of compression space, and the open hole has a large compression space. The teeth at the bottom of the gasket begin to thicken, and the upper sides of the gasket begin to expand to both sides due to extrusion. When the opening amount is 0mm, the closed holes on both sides of the gasket contact surface have been basically compressed and compacted, the open holes are not compressed and compacted, and there is still some compression space.

When the opening amount is 0mm, for the three sections of section A, B and C, their open hole shapes are the same, and the closed hole of section C has not been completely compressed and compacted. This is because the closed hole area of section C is larger than that of section A and section B, resulting in a larger opening rate of section C ; for both A and D sections, the shape of their closed holes is circular, and the opening rate of section D is the highest among the three, resulting in the closed hole of section D is not fully compressed when the opening is 0mm. Therefore, it can be concluded that the area of the closed hole will affect the dense state of the closed hole.

6.2 The Influence of Different Cross Section Forms on Contact Stress

In this section, the displacement load is applied to the segment to control the opening amount of the gasket to be 0mm, the rubber hardness to be 70, and the contact stress of the gasket-pad contact surface and the gasket-seal groove contact surface is extracted. The sections with the same type of open holes are divided into one group, and the six sections are divided into two groups. A, B, and C are a group, and D, E, and F are a group. The stress distribution diagram of the gasket along the contact surface is shown in Figure 11.

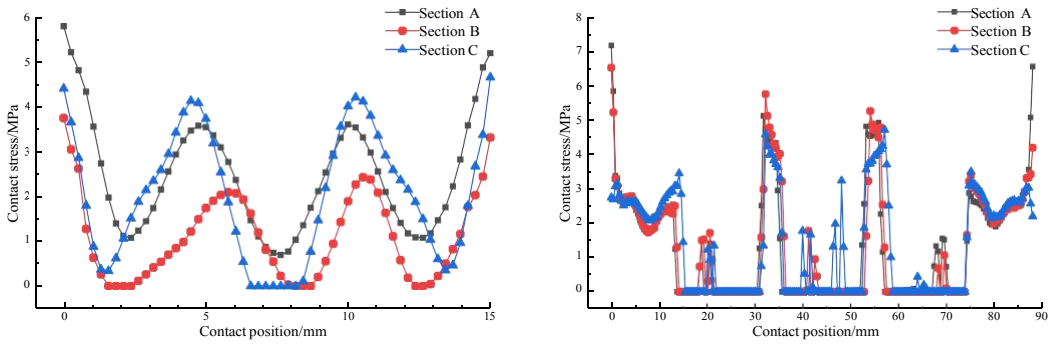

(a) Gasket-gasket contact surface (b)Gasket-Groove contact surface

Figure 11. Section A,B,C gasket along the contact surface stress distribution diagra

It can be seen from Figure 11 that the contact stress of the gasket-pad contact surface fluctuates greatly with the change of the contact position, and the peak value mostly occurs between the holes. The holes have a weakening effect on the contact stress, and the denser the holes are compressed, the greater the corresponding contact stress. Therefore, in the design process of the gasket, it should be ensured that the gasket hole can be completely compressed under the maximum compression amount, and the waterproof performance of the gasket can reach the maximum value.

It can be seen from Figure 11 that the contact stress of the gasket-pad contact surface changes with the change of the contact position, and the fluctuation trend of the six sections is basically the same. The stress on both sides of the contact stress at the contact surface of the six cross-section gasket-seal gasket is larger, and the contact stress in the middle part is ups and downs, but it does not exceed the contact stress at the edge of the contact surface ; among the six sections, the peak contact stress of section A, B and C in the middle part of the gasket-sealant contact surface is 60 and above the contact stress on both sides of the contact surface, while the peak contact stress of the middle part of

the other sections is 55 % and below the contact stress on both sides of the contact surface. Once the water pressure breaks through the edge contact part, the contact position of the middle part is not enough to maintain the overall waterproof performance of the gasket. In the case of 0mm dislocation, the deformation of the contact surface is basically symmetrical.

7. Conclusion

This study conducted a comprehensive numerical simulation and data-driven analysis to investigate the deformation characteristics and contact stress distribution of six different gasket cross-sections. Based on the simulation results and quantitative data analysis, the following conclusions can be drawn:

Under the same material hardness conditions, the average contact pressure at the gasket-pad interface is consistently lower than that at the gasket-groove interface. Among all contact surfaces, the gasket-gasket interface exhibits the highest average contact pressure, which plays a dominant role in determining the overall waterproofing performance, especially in scenarios without segment misalignment. Among the six evaluated sections, Section A demonstrates the best waterproofing performance, characterized by a stable and consistent growth trend in average contact stress under increasing compression displacement. This makes Section A the most suitable choice for practical engineering applications.The introduction of AI-assisted analysis techniques, including contact stress pattern recognition and multi-scenario performance prediction, offers significant potential for further optimizing gasket design.AI models trained on historical simulation data can improve the accuracy of stress distribution prediction, detect potential local weak points, and accelerate the iterative design process.

References

[1] Zhao Yunchen, Xiao Longge, Liu Zhaowei, et al. Experi ment Study and Design on the Watertight Seal for Reinforced Concrete Segment Joint of Wuhan Yangtze River Tunnel[J]. Tunnel Construction, 2008, 124(05): 570-575.

[2] Lu Ming, Cao Weibiao, Zhu Zuxi. Waterproofing design of extra - large diameter shield – driven tunnel[J]. China Building Waterproofing, 2008, 159(04): 17-21.

[3] Zhao Ming, Ding Wenqi, Peng Yicheng, et al. Experimental Study on the Reliability of Shield Tunnel Segment Joints to Remain Watertight Under High Water Pressure[J]. Modern Tunnelling Technology, 2013, 50(03): 87-93.

[4] TUO Yongfei, SHU Heng, GUO Xiaohong, et al. Design and experimental study on waterproof gasket of large-diameter shield tunnel under ultra high water pressure[J]. Chinese Journal of Geotechnical Engineering, 2013, 35(S1): 227-231.

[5] Zhong Xiaochun, Qin Jianshe, Zhu Wei, et al. Durability Tests and Analysis on the Waterproof Material for Joint Seam of Shield Tunnel[J]. Chinese Journal of Underground Space and Engineering, 2011, 7(02): 281-285.

[6] Wu Zhenzhi, Yang Linde, Ji Qianqian, et al. Experimental Study on Stress Relaxation of Waterproof Gasket of River-Crossing Shield Tunnel[J]. Journal of Building Materials, 2009, 12(05): 539-543.

[7] Gong Chenjie, Ding Wenqi. Waterproof Properties of Elastic Sealing Gaskets Used in Segmental Joints of Large-diameter Underwater Shield Tunnels: Design Methodology and Engineering Guidance[J]. Tunnel Construction, 2018,38(10):1712-1722.